Supplementary Information (SI) for Journal of Materials Chemistry C.

Supplementary Materials

Intrinsic piezoresistive mechanism of conductive porous nano composites with linearity assumption: Theory and experimental analysis

Yu Duan, Hua An, Weigao Wang, Chao Shang, Jianpeng Zhang *, Zhengchun Peng *

Center for Stretchable Electronics and Nano Sensors, Key Laboratory of Optoelectronic Devices and Systems of Ministry of Education, College of Physics and Optoelectronic Engineering, Shenzhen University, Shenzhen 518060, China.

******To whom correspondence should be addressed. zhangjp@szu.edu.cn & zcpeng@szu.edu.cn*

S1 Sample fabrication

Hierarchical porous piezoresistive nanocomposites (PPNs) were fabricated via a modified sacrificial NaCl templating method [Zhang et al., Adv. Theory Simul., 2021, 4, 210016] as depicted in Supplementary Figure S1. Specifically, thermoplastic polyurethane (TPU, Elastollan® 1185A, BASF) was dissolved in N,N-dimethylformamide (DMF, anhydrous, ≥99.8%, Aladdin) at 1:2 mass ratio under mechanical stirring at 60 °C for 4 hours. Carbon black (SUPER P Li, TIMCAL) was dispersed in ethyl acetate (EAC, 99.5%, Aladdin) via probe sonication (JY92-IIDN, SCIENTZ, 180W) for 30 minutes to enhance dispersion uniformity. Sodium chloride (NaCl, analytical grade, 99.5%) was ground using a planetary ball mill (F-P400, FOCUCY) for 2 hours and sieved to obtain microparticles with a median size of approximately 25 μm, serving as the sacrificial template. For slurry formulation, the TPU/DMF solution, CB/EAC dispersion, and NaCl microparticles were mixed at designed weight ratios to achieve final CB volume fractions (ϕ_c) of 5, 10, and 14 vol% (relative to the solid TPU+CB composite). The mixture was then homogenized via a double-blade planetary vacuum mixer (HM800, HASAI) at 800 rpm for 30 minutes under vacuum to obtain a homogeneous precursor slurry. This slurry was cast onto a clean glass plate using a doctor blade with a 1.0 mm gap, followed by solvent evaporation and curing in a ventilated oven at 80 °C for 6 hours to solidify the composite film. Subsequently, the sodium chloride template was removed by immersing the film in deionized water at 60 °C for 12 hours, with the water refreshed every 2 hours, resulting in a porous TPU/CB structure. The leached porous sheets were then dried in a vacuum oven at 60 °C for 12 hours to remove residual moisture. Finally, the sheets were precisely cut into test specimens with dimensions of 10 × 10 × 1 mm^3 (length × width × thickness) for electrical characterization using a precision laser cutter.

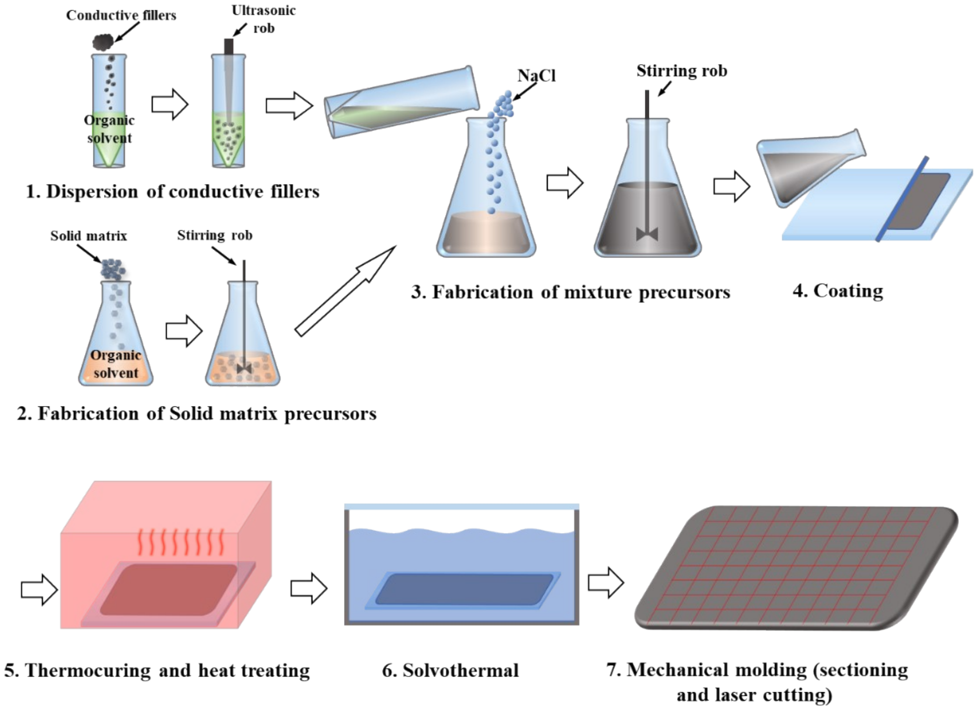

Figure S1 Fabrication process of PPN specimens

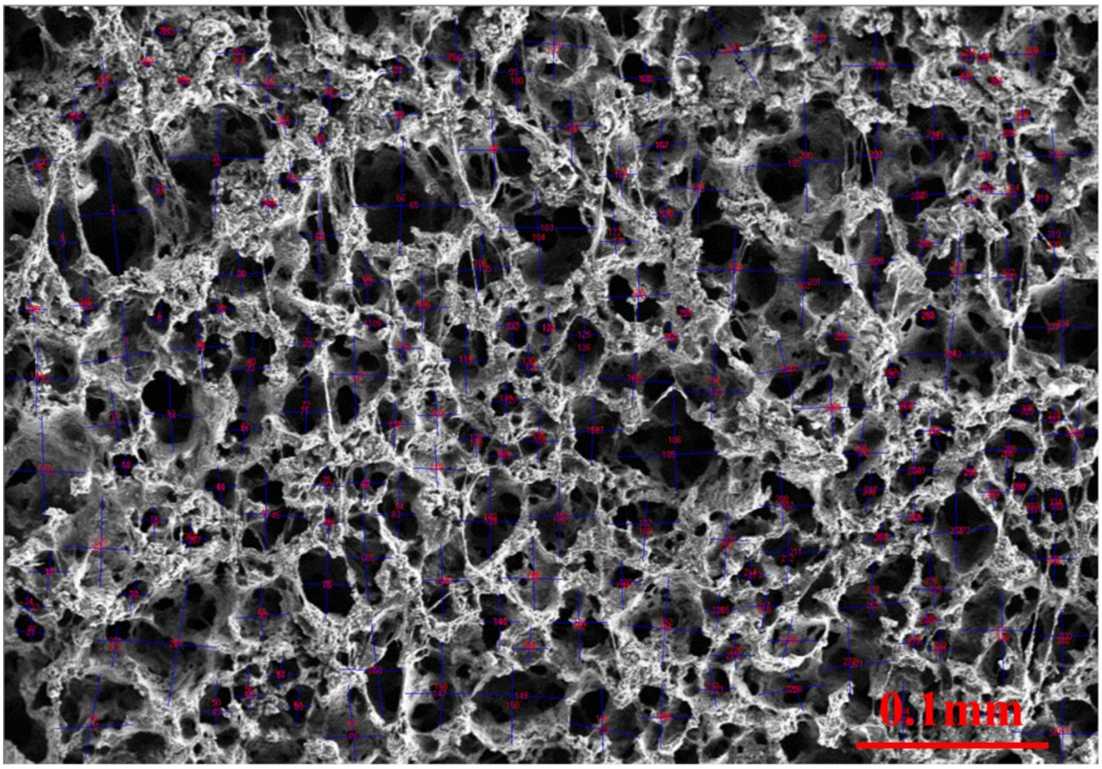

Figure S2 The measurement of the distribution of porous structure based on image recognition technology

S2. Material characterization

To examine the microscopic features and deformation of microstructures, a field emission scanning electron microscope (SEM) model Supra 55 by ZEISS is used. For evaluating the piezoresistive properties, a measurement system is established by combining a universal material testing machine (model E1000 by Instron) with a digital multimeter (model 34465A by Keysight). This setup allows for the measurement of stress-strain relationships and resistance-strain relationships. The bulk resistance of the PPNs was measured using the four-wire (Kelvin) method. This method employs two separate pairs of leads: one pair (Force+, Force-) to inject a constant current (I) through the sample, and an independent pair (Sense+, Sense-) to measure the voltage drop (V) directly across it. Because the voltage sensing circuit has very high input impedance, negligible current flows through it. Therefore, the voltage measurement excludes the parasitic voltage drops across the lead wires and contact interfaces, yielding a precise measurement of the intrinsic bulk resistance (R = V/I). This setup, which effectively eliminates contact resistance effects (L. J. van der Pauw,1958), is depicted in Figure S3.

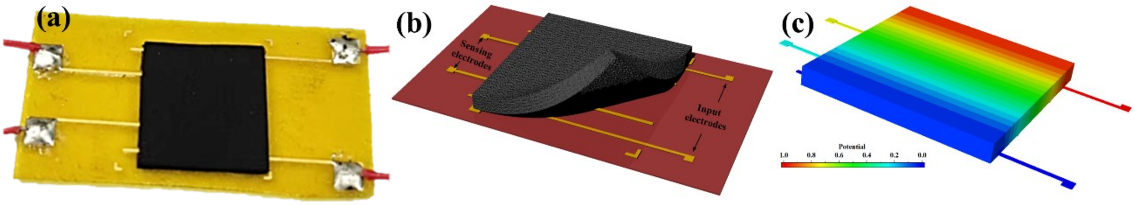

Figure S3 PPN sample and FPC of four-wires method

S3 adaptive moment estimation (ADAM) optimization algorithm of the fitting procedure

Machine learning has become a commonly employed approach in the field of science and engineering to confirm unknown parameters, particularly through the optimization of scalar parameterized objective functions that require maximization or minimization with respect to their parameters (Kingma and Ba, 2014). To establish a gradient descent path for the aforementioned optimization requirement, a differentiable cost function is proposed - consisting mainly of the discrepancy between true values and those obtained via machine learning. Numerous optimization algorithms have proven efficient and effective in addressing this task, including stochastic gradient descent (SGD), AdaGrad, RMSProp, and Adam. The latter combines the benefits of the first two algorithms, being invariant to gradient rescaling, adaptive to stepsizes, and capable of working with sparse gradients. Flow processes of the Adam optimization algorithm are illustrated in the following figure, showcasing its aptitude in computing pivotal parameters for analytical models based on experimental data.

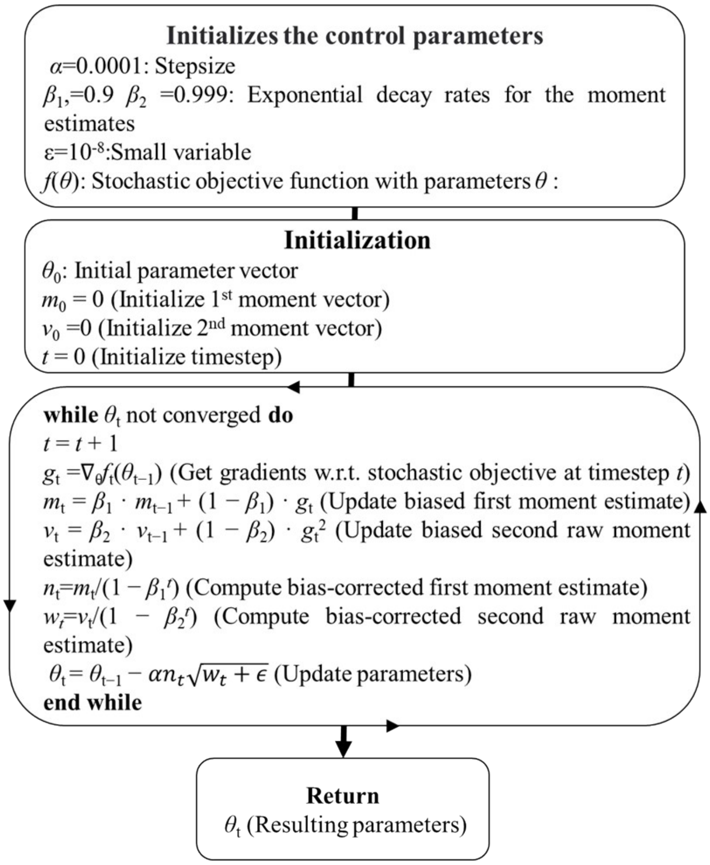

Figure S4 Flow-process diagram of Adam neural network optimization algorithm**.**

S4 Experimental verification of analytical model

We fabricated a GA model unit using a 3D printing process to experimentally validate the proposed analytical model. The printed unit was made of a conductive TPU filament with a diameter of 3mm and a conductivity of 1058.4 (Ω•m). The 3D printer utilized a thermosetting type with a nozzle size of 1.75mm. The resulting 3D model, as shown in Figure S4a, was subjected to pressure-resistance measurements using the aforementioned testing equipment. The dimensions of the printed unit were determined based on the aspect ratio of the strut structure p=0.183, yielding a value of 0.128. By further computations utilizing the unit's size (40×40×40mm), an effective resistivity of 218.22 (kΩ•m) was obtained, which is much higher than the resistivity of porous materials (0.2~10Ω•m). Consequently, by substituting this value into Equation 7, the estimated carbon black content of the material was found to be approximately 1.37v%. While fitting the theoretical formula (ξ~0.015), the analysis results exhibited a similar trend to the experimental results. However, significant deviations in specific values were observed due to substantial disparities between the structural formation during the 3D printing process and that of porous materials. Consequently, accurately fitting the experimental values using the proposed formula proved challenging.

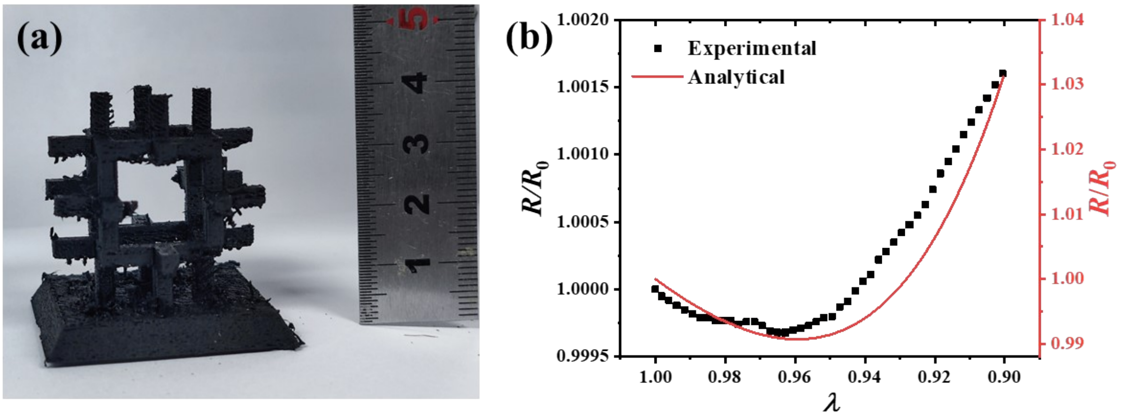

Figure S5 (**a**) 3D printed GA unit and (b) a comparison of the piezoresistive experimental results obtained from the GA unit with the corresponding analytical results.

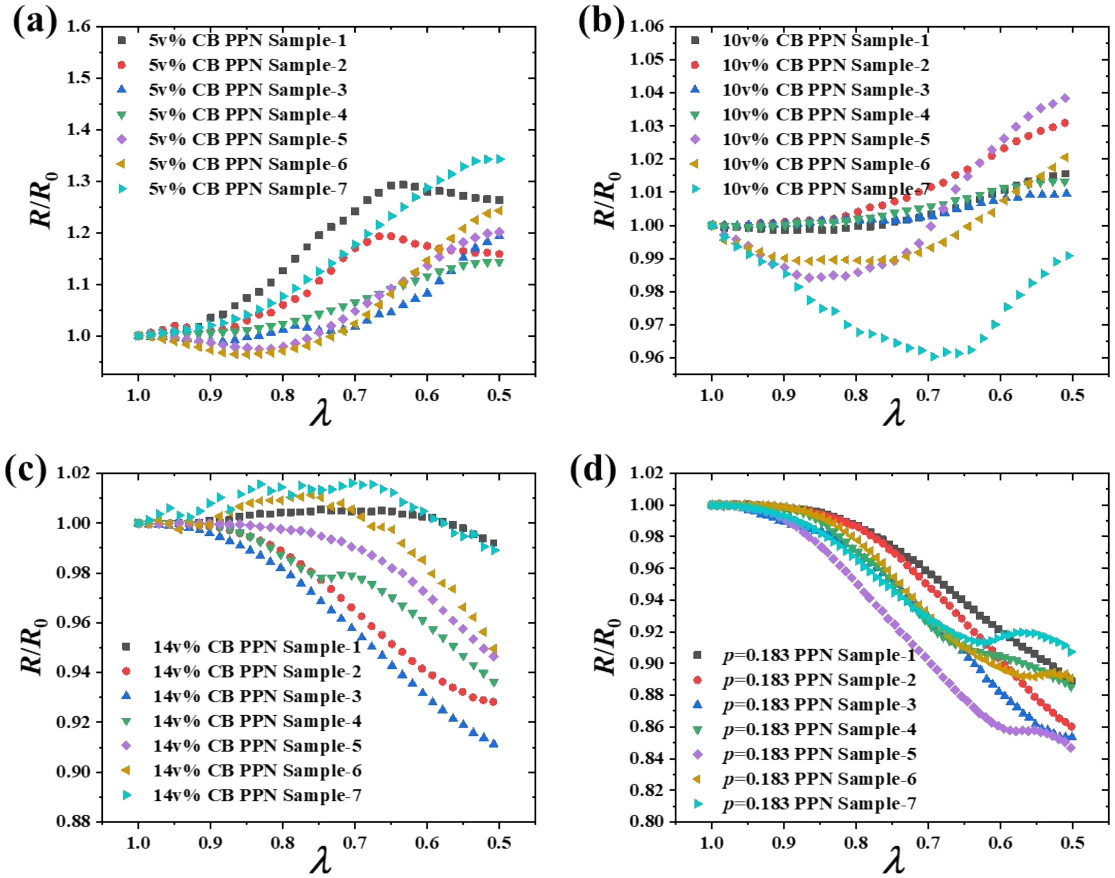

Figure S6 Experimental results of the piezoresistive measurements on samples categorized based on carbon black content and relative density. Experimental curves of PPN with different content CB (*p*=0.224) (**a, b, c**) and relative density (ϕ_c=14v%) (**c**, **d**).

S5 Finite element analysis (FEA) and its User defined material subroutine (UMAT) of piezoresistive composites

In order to confirm the piezoresistive behaviors within porous nanocomposite, finite element analysis (FEA) is applied (Zhang et al., 2021). However, the lack of piezoresistive material modules make it difficult to describe the electrical behaviors of piezoresistive composite under deformation. Thus, User defined material subroutine (UMAT) is established to describe the piezoresistive behaviors. First, based on Ezquerra model (Ezquerra et al., 1990), the conductivity vector (***COND***) can be expressed as a function about strain vector (***NE***)

$$\boldsymbol{COND}=\boldsymbol{COND0}\times \mathrm{EXP}(-\mathrm{MT}\times(1+\boldsymbol{NE}+{}^{SE^{2}/2X})),\qquad \text{(S3.1)}$$

with ***COND0*** as original conductivity vector, *MT* as electromechanical parameter depending on conductive fillers. Thus, the heat flux vector (***FLUX***) and the heat flux vector with respect to the spatial gradients of temperature (***DFDG***) can be written as

$$\boldsymbol{FLUX}=-\boldsymbol{COND}\times\boldsymbol{DTEMDX},\qquad \text{(S3.2)}$$

$$\boldsymbol{DFDG}=-\boldsymbol{COND},\qquad \text{(S3.3)}$$

with ***DTEMDX*** as spatial gradients of temperature. Moreover, in order to the strain filed during the deformation of the composite, user subroutine to redefine field variables at a material point (USDFLD) is used to combine with UMAT program(**Appendix** PHUMAT.for).

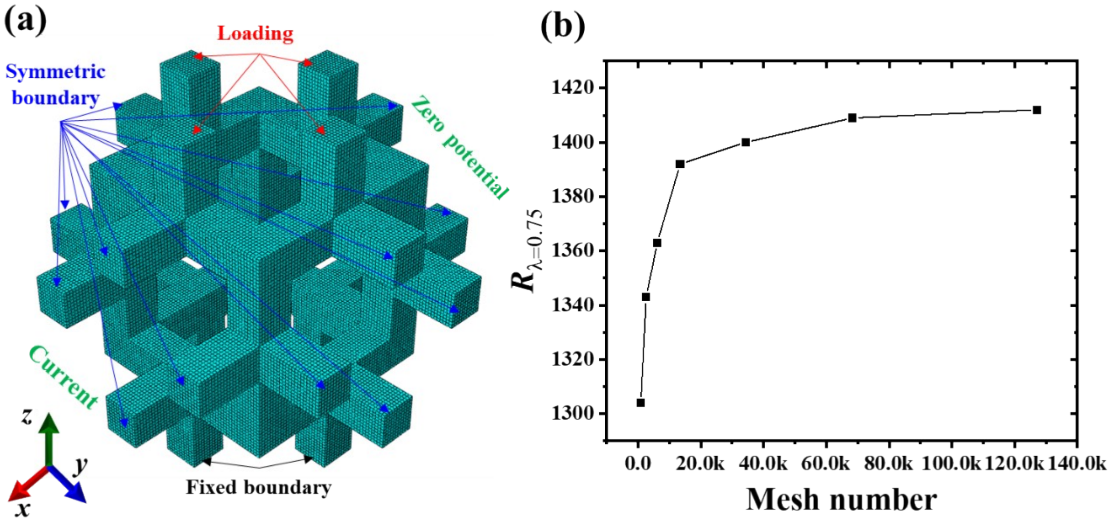

Figure S7 Mesh models of the GA cell for PPN (**a**) and convergence graph of resistance against mesh number (**b**)

Appendix PHUMAT.for

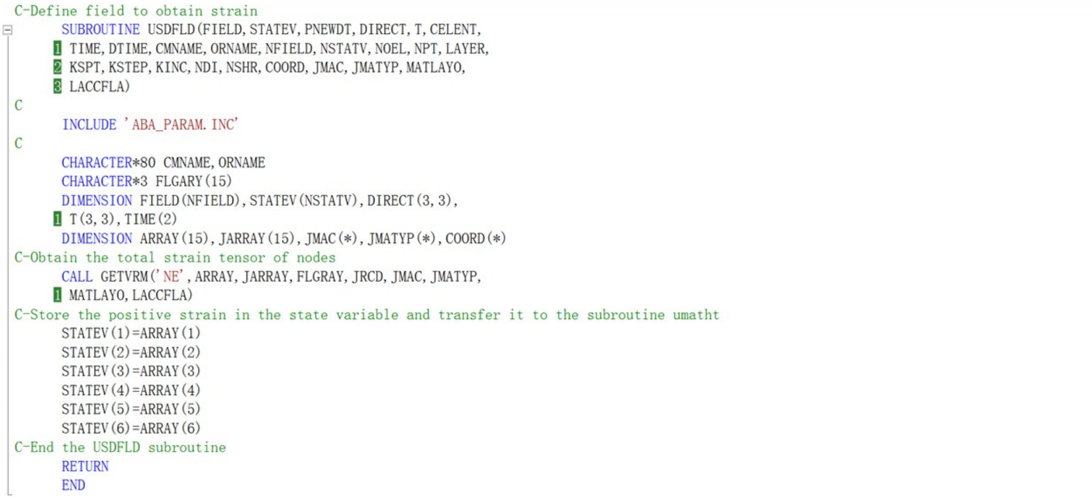

```
C-Define field to obtain strain
      SUBROUTINE USDFLD(FIELD,STATEV,PNEWDT,DIRECT,T,CELENT,
     1 TIME,DTIME,CMNAME,ORNAME,NFIELD,NSTATV,NOEL,NPT,LAYER,
     2 KSPT,KSTEP,KINC,NDI,NSHR,COORD,JMAC,JMATYP,MATLAYO,
     3 LACCFLA)
C
      INCLUDE 'ABA_PARAM.INC'
C
      CHARACTER*80 CMNAME,ORNAME
      CHARACTER*3 FLGARY(15)
      DIMENSION FIELD(NFIELD),STATEV(NSTATV),DIRECT(3,3),
     1 T(3,3),TIME(2)
      DIMENSION ARRAY(15),JARRAY(15),JMAC(*),JMATYP(*),COORD(*)
C-Obtain the total strain tensor of nodes
      CALL GETVRM('NE',ARRAY,JARRAY,FLGRAY,JRCD,JMAC,JMATYP,
     1 MATLAYO,LACCFLA)
C-Store the positive strain in the state variable and transfer it to the subroutine umatht
      STATEV(1)=ARRAY(1)
      STATEV(2)=ARRAY(2)
      STATEV(3)=ARRAY(3)
      STATEV(4)=ARRAY(4)
      STATEV(5)=ARRAY(5)
      STATEV(6)=ARRAY(6)
C-End the USDFLD subroutine
      RETURN
      END
```

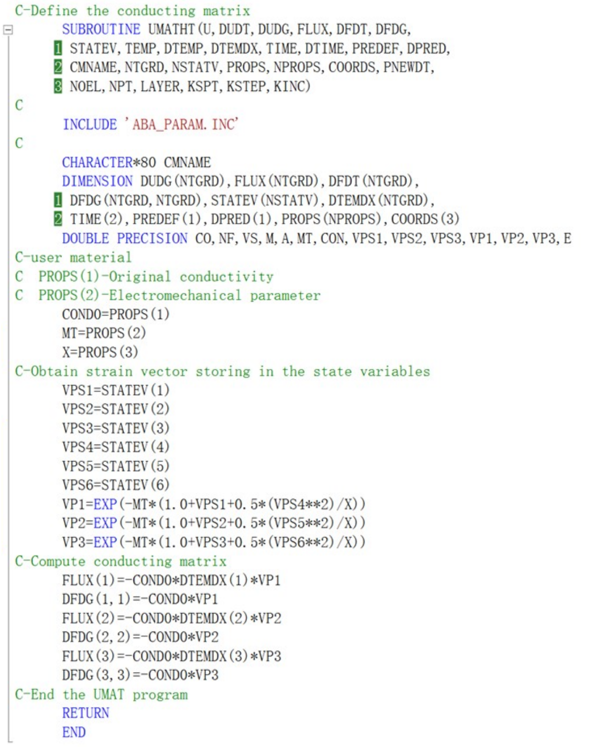

```
C-Define the conducting matrix
      SUBROUTINE UMATHT(U,DUDT,DUDG,FLUX,DFDT,DFDG,
     1 STATEV,TEMP,DTEMP,DTEMDX,TIME,DTIME,PREDEF,DPRED,
     2 CMNAME,NTGRD,NSTATV,PROPS,NPROPS,COORDS,PNEWDT,
     3 NOEL,NPT,LAYER,KSPT,KSTEP,KINC)
C
      INCLUDE 'ABA_PARAM.INC'
C
      CHARACTER*80 CMNAME
      DIMENSION DUDG(NTGRD),FLUX(NTGRD),DFDT(NTGRD),
     1 DFDG(NTGRD,NTGRD),STATEV(NSTATV),DTEMDX(NTGRD),
     2 TIME(2),PREDEF(1),DPRED(1),PROPS(NPROPS),COORDS(3)
      DOUBLE PRECISION CO,NF,VS,M,A,MT,CON,VPS1,VPS2,VPS3,VP1,VP2,VP3,E
C-user material
C  PROPS(1)-Original conductivity
C  PROPS(2)-Electromechanical parameter
      COND0=PROPS(1)
      MT=PROPS(2)
      X=PROPS(3)
C-Obtain strain vector storing in the state variables
      VPS1=STATEV(1)
      VPS2=STATEV(2)
      VPS3=STATEV(3)
      VPS4=STATEV(4)
      VPS5=STATEV(5)
      VPS6=STATEV(6)
      VP1=EXP(-MT*(1.0+VPS1+0.5*(VPS4**2)/X))
      VP2=EXP(-MT*(1.0+VPS2+0.5*(VPS5**2)/X))
      VP3=EXP(-MT*(1.0+VPS3+0.5*(VPS6**2)/X))
C-Compute conducting matrix
      FLUX(1)=-COND0*DTEMDX(1)*VP1
      DFDG(1,1)=-COND0*VP1
      FLUX(2)=-COND0*DTEMDX(2)*VP2
      DFDG(2,2)=-COND0*VP2
      FLUX(3)=-COND0*DTEMDX(3)*VP3
      DFDG(3,3)=-COND0*VP3
C-End the UMAT program
      RETURN
      END
```

Appendix A _Detailed Mathematical Derivations and Parament Explanations

A.1 Derivation of the reaction moment M and rotation β_0:

For the Timoshenko beam, the moment-curvature relationship $M = EI\frac{d\varphi}{dx}$, integrating the moment expression $M_T|_{x \le 0} =- M_0 + \frac{F}{2}(x + L_{t1}),L_{t1} = \frac{l\tan\alpha}{2}$ from Eq. (9):

$$EI\frac{d\varphi}{dx} =- M_0 + \frac{F}{2}(x + L_{t1}) \tag{A.1.1}$$

Integrating once with respect to x:

$$\varphi_T(x) = \frac{1}{EI}\left[- M_0x + \frac{F}{4}(x + L_{t1})^2\right] + C_1 \tag{A.1.2}$$

Applying the boundary condition $\varphi_T(0) = 0$ yields $C_1 = \frac{1}{EI}\left[- \frac{F}{4}(L_{t1})^2\right] = - \frac{F{L_{t1}}^2}{4EI}$.

$$\varphi_T(x) = \frac{1}{EI}\left[- M_0x + \frac{F}{4}(x^2 + 2L_{t1}x)\right] \tag{A.1.3}$$

Applying $\varphi_T(- L_{t1}) = \beta_0$ gives:

$$\beta_0 = \frac{M_0L_{t1}}{EI} - \frac{F{L_{t1}}^2}{4EI} \tag{A.1.4}$$

For the Timoshenko beam, the moment-curvature relationship $M = EI\frac{d\varphi}{dy}$, integrating the moment expression of the vertical beam expression $M_V(y)|_{0 \le y \le \frac{l}{2}} = M_0$ from Eq. (9):

$$\varphi_V(y) = \frac{M_0}{EI}y + C_2 \tag{A.1.5}$$

Applying $\varphi_V(0) = 0$ yields $C_2 = 0$. Applying $\varphi_V\left(\frac{l}{2}\right) =- \beta_0$ gives:

$$- \beta_0 = \frac{M_0}{EI} \cdot \frac{l}{2} \Rightarrow \beta_0 =- \frac{M_0l}{2EI} \tag{A.1.6}$$

Substituting $\beta_0 = \frac{M_0L_{t1}}{EI} - \frac{F{L_{t1}}^2}{4EI}$ gives:

$$\begin{cases} M_0 = \dfrac{\tan\alpha^2Fl}{8(1 + \tan\alpha)} \\ \beta_0 = \dfrac{Fl^2\tan\alpha^2}{16(1 + \tan\alpha)EI} \end{cases} \tag{10}$$

$$\varphi_T(x) = \frac{F}{4EI}\left[x^2 - \frac{l(2 + \tan\alpha)\tan\alpha}{2(1 + \tan\alpha)}x\right] \tag{11}$$

A.2 Derivation of the overall compressive strain

Solving the governing equation (Eq. 8) with the boundary conditions (Eq. 9) and the solved M_0 and β_0, the deflection of the transverse beam $w_T(x)$ can be obtained. The overall compressive strain λ of the unit cell is defined as the total vertical displacement normalized by the original height l. It comprises two parts: the displacement due to bending of the transverse beams ($2w_T(0)/l$) and the displacement due to shear deformation of the beams. The final expression is:

$$\lambda = 1 - \frac{2w_T(0)}{l} - \frac{F\tan\alpha}{4\kappa GA} = 1 - \left(\frac{Fl^2\tan^3\alpha(4 + \tan\alpha)}{96EI(1 + \tan\alpha)}\right) - \frac{3F\tan\alpha}{4\kappa GA} \tag{12}$$

Derivation of the Deflection Distribution w

The deflection slope equation for a Timoshenko beam, which incorporates the effect of transverse shear deformation, is given by:

$$EI\varphi'' + \kappa GA(w' - \varphi) = 0 \tag{6}$$

$$\frac{dw}{dx} = \varphi(x) + \frac{V}{\kappa GA} \tag{A.2.1}$$

where $\varphi(x)$ is the rotation due to bending, V is the shear force, κ is the shear correction factor, G is the shear modulus, and A is the cross-sectional area.

For the beam segment under consideration, the shear force is constant: $V = F/2$. Substituting the expression for $\phi(x)$(derived from the moment-curvature relationship) yields:

$$\frac{dw}{dx} = \frac{1}{EI}\left\{ - Mx + \frac{F}{4}(x^2 + 2L_{t1}x)\right\} + \frac{F}{2\kappa GA} \tag{A.2.2}$$

Integrating Equation (A.2.1.1) with respect to x gives the deflection distribution:

$$w(x) = \int\left[\frac{1}{EI}\left\{ - M_0x + \frac{F}{4}(x^2 + 2L_{t1}x)\right\} + \frac{F}{2\kappa GA}\right]dx \tag{A.2.3}$$

Performing the integration:

$$w(x) = \frac{1}{EI}\left\{ - \frac{M_0}{2}x^2 + \frac{F}{12}x^3 + \frac{FL_{t1}}{4}x^2\right\} + \left[\frac{F}{2\kappa GA}\right]x + C_3 \tag{A.2.4}$$

where C_3 is the constant of integration.

Applying the boundary condition at the fixed support, $w_T(- L_{t1}) = 0$, and substituting $x = - L_{t1}$ into Equation (A.2.2):

$$0 = \frac{1}{EI}\left\{ - \frac{M_0}{2}(- L_{t1})^2 + \frac{F}{12}(- L_{t1})^3 + \frac{FL_{t1}}{4}(- L_{t1})^2\right\} + \left[\frac{F}{2\kappa GA}\right](- L_{t1}) + C_3 \tag{A.2.5}$$

Solving for C_3:

$$C_3 = \frac{FL_{t1}}{2\kappa GA} - \frac{1}{EI}\left[\frac{M_0}{2}L_{t1}^2 - \frac{F}{6}L_{t1}^3\right] = \frac{Fl\tan\alpha}{4\kappa GA} + \frac{Fl^3\tan^3\alpha(\tan\alpha + 4)}{192EI(1 + \tan\alpha)} \tag{A.2.6}$$

The deflection at the connection point with the vertical beam ($x = 0$) is obtained by substituting $x = 0$ and the expression for C_3 into Equation (A.2.2):

$\omega(0) = C_3$

$$w(0) = \frac{Fl\tan\alpha}{4\kappa GA} + \frac{Fl^3\tan^3\alpha(\tan\alpha + 4)}{192EI(1 + \tan\alpha)} \tag{A.2.7}$$

$$\lambda = 1 - \frac{2w_T(0)}{l} - \frac{F\tan\alpha}{4\kappa GA} = 1 - \left(\frac{Fl^2\tan^3\alpha(4 + \tan\alpha)}{96EI(1 + \tan\alpha)}\right) - \frac{3F\tan\alpha}{4\kappa GA} \tag{12}$$

A.3 Derivation of the local deformation functions δ_T and δ_V:

$$\delta = 1 + \varepsilon + \frac{\gamma^2}{2\xi}. \tag{6}$$

The normal strain ε for the transverse beam arises from bending: $\varepsilon_T = z \cdot \frac{d\varphi_T}{dx} = z \cdot \frac{M_T(x)}{EI}$.

The shear strain is primarily considered in the transverse beam and is constant for a beam under pure shear: $\gamma_T = \frac{Q}{\kappa GA} = \frac{F}{2\kappa GA}$

The normal strain for the vertical beam includes axial compression and bending: .$\varepsilon_V = \frac{F}{EA} + y \cdot \frac{d\varphi_V}{dy} = \frac{F}{EA} + \frac{M_0}{EI}y$

Substituting these strain expressions into Eq. (6) gives the local deformation functions for the transverse and vertical beams, respectively:

$$\begin{cases} \delta_T = 1 + \dfrac{Fz}{EI}\left(\dfrac{l\tan\alpha(2+\tan\alpha) + 4x(\tan\alpha + 1)}{8(1+\tan\alpha)}\right) + \dfrac{1}{2\xi}\left(\dfrac{F}{2\kappa GA}\right)^2 \\ \delta_V = 1 + \dfrac{F}{EA} + \dfrac{Fl\tan^2\alpha(x+y)}{8(1+\tan\alpha)EI} \end{cases}, \tag{13}$$

Finally, by integrating the resistivity model Eq. (7) over the beam volume using $R = \int_l \left[\frac{1}{\iint_A \rho^{-1} dA}\right] dl$, the resistances of the transverse and vertical beams are obtained as expressed in Eq. (13).

A.4 Parameters of the Piezoresistive Model for PPNs

Table A1 summarizes all key parameters introduced in the theoretical model, along with their symbols, physical meaning, and origin. The parameters are grouped by their primary physical context to enhance clarity.

Table 1. Parameters of the piezoresistive model for PPNs

Group / Context	Parameter	Symbol	Physical Meaning & Role in the Model	Typical Origin / How Determined
1. Geometry & Structure	Relative density	p	Ratio of foam density to solid density (ρ_foam / ρ_solid). Scales the ligament dimensions in the Gibson-Ashby model.	Measured from sample mass and volume.
	Structural parameter	tan α	Ratio of transverse to vertical ligament length in the unit cell. Defines the cell geometry and deformation mode under compression.	Defined by the sacrificial template geometry (NaCl particle shape/size).

2. Solid Material Constitutive	Ligament Young's modulus	E	Young's modulus of the solid composite (TPU+CB) ligament. Governs the elastic bending response in the beam model.	Measured via tensile test on dense composite.
	Ligament shear modulus	G	Shear modulus of the solid composite. Governs the shear deformation in the Timoshenko beam model.	Calculated as $G = E / (2(1+\nu))$ or measured.
	Timoshenko shear coefficient	κ	Factor accounting for non-uniform shear stress distribution across the beam's rectangular cross-section.	Theoretical value, typically $\kappa = 5/6$ for a rectangular section [1].
3. Conductive Network	Tunneling constant	χ	Height of the potential barrier for electron tunneling between CB particles. Directly scales the exponential sensitivity of resistivity to inter-particle distance.	Fitted parameter, constrained by the slope of ln(R) vs. strain data.
	Porosity exponent	c	Exponent describing how porosity (p) amplifies the tunneling distance. Captures the effect of porous structure on network connectivity.	Fitted parameter, typically between 1 and 2 for open-cell foams.
	Geometric factor	n	Proportionality constant in the undeformed inter-particle distance d_0. Relates the composite's microstructure to the characteristic tunneling gap.	Fitted parameter, often close to 1.
	Crosslinking factor (Constraint efficiency factor)	ξ	**Phenomenological factor** quantifying the matrix's efficiency in constraining filler separation under shear strain (γ). A higher ξ indicates less network degradation for a given γ.	*Fitted parameter. Its variation with CB content and porosity provides indirect evidence for its physical basis (see Section 3.2).*
	Filler volume fraction	ϕ_c	Volume fraction of conductive filler (CB) in the solid composite. Inversely affects the initial inter-particle distance d_0.	Controlled during sample fabrication.
4. Viscoelasticity	Spring modulus (fast)	E_1	Elastic modulus of the Maxwell arm's spring, representing instantaneous bond distortion.	Obtained from fitting the quasi-static stress-strain curve or dynamic mechanical analysis (DMA).

	Spring modulus (slow)	E_2	Elastic modulus of the Kelvin-Voigt arm's spring, representing the resistance of entangled chains to rearrangement.	Fitted from stress relaxation or creep data.
	Dashpot viscosity (slow)	η_1	Viscosity of the Kelvin-Voigt arm's dashpot, representing the viscous resistance to chain motion.	Fitted from stress relaxation or creep data.
	Structural dashpot coefficient	η'	Phenomenological viscosity representing the rate of ligament shape recovery after large deformation.	Fitted from the time-dependent resistance recovery data (Fig. 8).

[1] Öchsner, A., *Classical Beam Theories of Structural Mechanics*, Springer, 2021.

Reference

Ezquerra, T.A., Kulescza, M., Cruz, C.S., Baltá-Calleja, F.J., 1990. Charge transport in polyethylene–graphite composite materials. Advanced Materials 2, 597-600.

Kingma, D.P., Ba, J., 2014. Adam: A Method for Stochastic Optimization. CORR abs/1412.6980.

Zhang, J., Wang, Z., Peng, Z., 2021. Analytical Model of the Piezoresistive Behavior of Highly Compressible Sensors Made of Microporous Nanocomposites. Advanced Theory and Simulations 4, 2100247.

L. J. van der Pauw, "A Method of Measuring Specific Resistivity and Hall Effect of Discs of Arbitrary Shape," Philips Research Reports, Vol. 13, February 1958, pp. 1-9